ENVIRONMENTAL RESEARCH
CLIMATE

OPEN ACCESS

RECEIVED
23 January 2026

REVISED
29 March 2026

ACCEPTED FOR PUBLICATION
22 May 2026

PUBLISHED
22 June 2026

PAPER

How and why do Greenland blocking patterns vary significantly between different summer months?

Linh N Luu[1,2,*], **Edward Hanna**[1], **Tim Woollings**[3], **Xavier Fettweis**[4], **James A Screen**[5], **Stephanie Hay**[5] and **Jennifer Catto**[5]

[1] Department of Geography, University of Lincoln, Lincoln, United Kingdom
[2] Now at Sustainable Law Programme, Smith School of Enterprise and Environment, University of Oxford, Oxford, United Kingdom
[3] Atmospheric, Oceanic and Planetary Physics, Department of Physics, University of Oxford, Oxford, United Kingdom
[4] Laboratory of Climatology, Department of Geography, SPHERES Research Unit, University of Liège, Liège, Belgium
[5] Department of Mathematics and Statistics, University of Exeter, Exeter, United Kingdom
[*] Author to whom any correspondence should be addressed.

E-mail: linh.luu@smithschool.ox.ac.uk

Keywords: atmospheric blocking, greenland blocking, wave propagation, atmospheric dynamics, self organising map

Supplementary material for this article is available online

Abstract

Greenland atmospheric blocking, a persistent anticyclonic pattern, strongly influences local and regional weather and climate. It is known to significantly exacerbate Greenland ice sheet melt and mass loss in summer as well as influence atmospheric conditions over the North Atlantic. Greenland blocking has been observed to increase in intensity since the summer of 2000s, but this trend has partly reversed after 2012. This decadal variability is highly correlated with the negative phase of the North Atlantic Oscillation (NAO), the dominant pattern of climate variability in the North Atlantic. However, summer NAO shows different temporal variation in June in comparison with later summer months, i.e. July and August. In this study, we analyse the individual summer months in turn to evaluate differences between their respective spatial patterns of Greenland blocking events. We use different approaches including a self-organising map to evaluate individual blocking days, and an event-based analysis to assess the development of blocking events over the course of 7 d. The results show that spatial patterns of Greenland blocking are similar between July and August but are distinctly different in June. In particular, Greenland blocking in June is strongly related to cyclonic wave breaking over the eastern Atlantic. Our analysis using wave activity flux of the zonally varying mean flow reveals a distinct pattern of wave energy and pseudo-momentum associated with cyclonic wave breaking prior to Greenland blocking high anomalies in June, in contrast to the other two summer months. This might partially explain the difference in the spatial patterns and evolution of blocking in June compared with July and August.

1. Introduction

Atmospheric blocking, persistent large-scale anticyclonic circulation anomalies, occurring in mid-to-high latitude regions can lead to extreme surface weather, not only in the blocking regions but also upstream and downstream of these (Woollings *et al* 2018, Lupo 2021, Kautz *et al* 2022). The phenomenon was first documented as 'blocking action' by Elliott and Smith (1949) and since then its mechanism and characteristics have been explored using different theories. For example, a well-known perspective on blocking is its association with Rossby wave breaking, defined by the reversal of the meridional potential temperature gradient on the dynamical tropopause (Pelly and Hoskins 2003, Altenhoff *et al* 2008, Weijenborg *et al* 2012). In addition, blocking can be viewed as a slowing or stalling of energy dispersion of an initial single wave packet during its onset and is maintained its by interaction with synoptic-scale transient eddies (Yeh 1949, Luo 2000). Other studies explain blocking as analogous to a traffic jam in the context of wave activity flux (WAF) convergence on the westerly mean flow (Takaya and Nakamura 2001,

Nakamura and Huang 2018, Shi and Nakamura 2021), although—due to the relative position of the jet stream—this concept is probably more applicable to midlatitudes rather than high-latitude blocking. While most attention has focused on barotropic wave processes, baroclinic energy conversion can play a strong role in blocking formation, including over Greenland in summer (Martineau *et al* 2022). From a potential vorticity (PV) perspective, the onset and maintenance of blocking are closely related to stationary negative PV anomalies associated with the warm conveyor belt (a warm, moist airstream that emanates in an extratropical cyclone warm sector and moves upwards and polewards) and moist processes upstream of the blocking region (Hoskins 1997, Schwierz *et al* 2004, Steinfeld and Pfahl 2019, Hauser *et al* 2023, 2024, Mathews and Czaja 2024). However, dry wave dynamics can itself produce blocking with similar size, intensity and duration to observed blocking by efficiently feeding upper-level low PV-air from lower latitudes poleward towards the blocking region, although blocking frequency is significantly lower in the absence of moist processes (Deshmukh *et al* 2025). The temporal development of blocking and how it is influenced by climate change can also be studied using a nonlinear multiscale interaction model, which can account for the nonlinearity and high-order dispersion of a slowly varying zonal mean flow (Luo *et al* 2025). However, the dominant mechanism of blocking onset and maintenance, and blocking interaction with mean flow and high frequency eddies may be explained by different theories for different regions (Nakamura *et al* 1997, Drouard and Woollings 2018, Miller and Wang 2022, Ma and Liang 2023). Hence, the underlying physical causes of blocking, and how blocking responds to, and influences broader-scale climate, still require further investigation, especially in terms of connecting the daily weather timescale with longer-term climate change (Woollings *et al* 2018).

Due to the seasonality of the atmosphere and the ocean conditions, blocking also varies between seasons and regions. Blocking in summer and autumn is generally less strong and less frequent than in winter and spring (Cheung *et al* 2013, Woollings *et al* 2018, Lupo 2021, Nabizadeh *et al* 2021). Over the northern hemisphere, long (10–13 d) and very long (>14 d) blocking events tend to happen more frequently in January, May, and June compared to other calendar months (Drouard *et al* 2021). Summer blocking over Greenland can be intensified in association with precursor cyclones over the North Atlantic (McLeod and Mote 2015). Winter Greenland blocking characteristics can be reciprocally modulated by the variability of the stratospheric polar vortex (SPV, Hanna *et al* 2024), however, blocking-SPV coupling is suppressed in summer due to prevailing easterly wind in the stratosphere in that season (Zhang *et al* 2024), notwithstanding evidence of correlation between stratospheric warming in late spring and the summer North Atlantic Oscillation (NAO, Dunstone *et al* 2023), where the latter is inversely correlated with Greenland blocking. On a decadal timescale, Greenland blocking metrics generally agree well on a seasonal basis but show large divergence for summer, especially after 2005 (Wachowicz *et al* 2020). He *et al* (2018) show that summer blocking is more frequent but is less long-lived in response to the positive phase of land-sea thermal contrast (based on land-sea index) compared to the negative phase, while the response of winter blocking is opposite. Vishnupriya *et al* (2025) reveal that the frequency of interactions between the outflow of the warm conveyor belt, the associated tropospheric waveguide and blocking is much lower in the summer compared to other seasons.

Atmospheric blocking over Greenland, especially over the southern tip of Greenland and the Labrador Sea, tends to last longer (>9 d on average) than blocking over other regions (Davini *et al* 2012). These persistent Greenland blocking episodes have far-reaching impacts on extreme weather over much of the mid-to-high-latitude North Atlantic region. During summer, Greenland blocking can trigger record warm events and extreme melting of the Greenland Ice Sheet (GrIS), resulting in negative surface mass balance (SMB, i.e. snow accumulation minus the runoff of surface meltwater) due to the advection of warmer air from lower latitudes (McLeod and Mote 2016, Hermann *et al* 2020, Preece *et al* 2022). Blocking also amplifies downward longwave radiation over the interior northern part of the ice sheet by channelling moist airflow along the upstream flank, which generates cloud cover (Mattingly *et al* 2018). Delhasse *et al* (2018) suggest that GrIS SMB could decrease by a factor of two with a circulation change favouring blocking, compared with no circulation changes, under similar warming conditions. This enhanced GrIS melting can significantly add to regional and global sea-level rise (Fettweis *et al* 2013, Beckmann and Winkelmann 2023).

The balance of different blocking mechanisms varies between regions and depends on their seasonality (Woollings *et al* 2018). However, for Greenland blocking, this balance varies considerably within the summer season. According to a popular paradigm, Greenland blocking is closely related to the negative phase of the NAO (Feldstein 2007, Woollings and Hoskins 2008, Woollings *et al* 2008), although this link is weaker in summer than winter in some metrics (Dong *et al* 2013). However, the temporal variation of June summer NAO is different from the high summer months, e.g. July and August (Folland *et al* 2009). Sun *et al* (2024) show that combining all summer months without removing the seasonal cycle from each month produces a poorly defined spatial pattern of the first Empirical Orthogonal Function

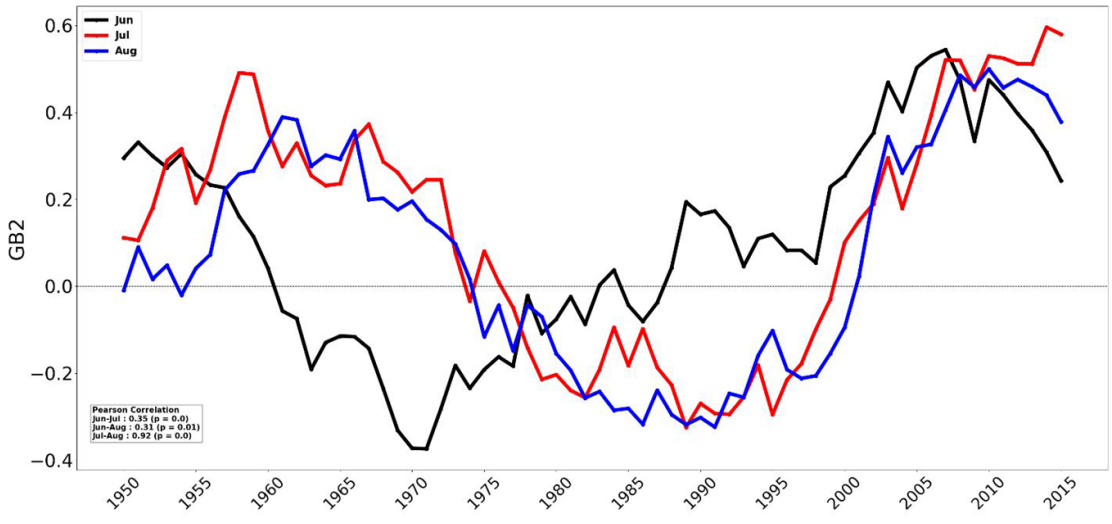

Figure 1. Timeseries of Greenland Blocking index (GB2) for three summer months (JJA) based on ERA5 from 1940–2024. All timeseries are smoothed by a 20-year running average. The detail of GB2 index and ERA5 data are given in section 2.

(EOF) of 500 hPa geopotential height over the North Atlantic region; this EOF1 normally resembles the NAO (e.g. Hall and Hanna 2018). This suggests a potential difference in the development and variation of Greenland blocking between June and the high summer months due to their seasonality. Indeed, time series of monthly Greenland Blocking index (GBI) GB2 (see section 2 for the definition of GB2) between July and August are highly correlated (Pearson correlation $\sim$ 0.92), while their correlations with June are much lower (0.35 and 0.31, respectively in figure 1). In addition, some studies on blocking climatology define a blocking year starting in July and lasting until June of the next year, with the blocking summer defined as July/August/September while June is the last month of spring (Wiedenmann *et al* 2002, Lupo *et al* 2019). This blocking year definition is based on the climatological seasonal cycle of blocking characteristics (Lupo and Smith 1995). In terms of impact, different pattern, locations and strength of Greenland summer blocking impose different effects on GrIS surface energy and mass balance, hence producing distinct melt patterns and intensities, with surface melt even reaching the top of the ice-sheet plateau in some cases (Preece *et al* 2022). Different GBI anomalies and their seasonal and interannual changes also have potentially different downstream effects on the North Atlantic atmospheric jet stream behaviour (Hanna *et al* 2018) and resulting midlatitude extreme weather. For example, a positive Greenland Blocking trend in summer since the 1990s tended to deflect the North Atlantic jet stream southwards of its normal summer position and contribute to some record wet summer weather and costly flooding episodes in England and Wales e.g. in 2007 and 2012 (Hanna *et al* 2017). Therefore, any potential differences in the spatial evolution of Greenland blocking among the three summer months could impose different impacts over large parts of the North Atlantic and Greenland regions. In this study, we address the question 'How and why do Greenland blocking patterns significantly vary between different summer months?'. We also discuss the impacts of these different Greenland blocking patterns on the NAO and downstream on precipitation patterns over western Europe. This introduction is followed by data and method descriptions in section 2, results and discussion in section 3 and a summary of the key findings in section 4.

2. Data and method

In this study, we use daily geopotential height, zonal and meridional wind components, air temperature and PV from pressure levels from the fifth generation ECMWF atmospheric reanalysis (ERA5, Hersbach *et al* 2020) to investigate the large-scale dynamics of Greenland blocking for individual summer months. These data are collected for the period of 1955–2024 because we notice that sea ice cover over the Arctic Ocean and its marginal seas, which have potential impact on Greenland blocking (Liu *et al* 2016, Sellevold *et al* 2022), remains constant for those years prior to 1955 in ERA5 (see supplementary figure S1). In addition, we use daily precipitation from the updated ensemble version of E-OBS with 0.1° horizontal resolution (Cornes *et al* 2018) to investigate the downstream impact of Greenland blocking over western Europe.

We use the normalised GBI (GB2, Hanna *et al* 2018), a metric measuring the ridge over Greenland, and the meridional gradient of flow index (D12, Davini *et al* 2012), a metric detecting the reversal of north–south height gradient and taking into account positive anomalies over Greenland, which are both computed based on 500 hPa geopotential height (z500) to define blocking days and events following the procedure described in Luu *et al* (2024). All blocking events determined by either GB2 or D12 using a 4 d persistence criterion are considered. If an event detected by GB2 has one or a few days overlapping with an event detected by D12, we merge them into one longer blocking event. This determines 81 (41 by GB2, 66 by D12 and 26 overlapping), 67 (39 by GB2, 51 by D12 and 23 overlapping) and 66 (44 by GB2, 46 by D12 and 24 overlapping) blocking events for June, July and August, respectively.

To facilitate a comparison for all blocking days of an individual month to others in section 3.1, we use the self-organising map (SOM) method to cluster the ERA5 z500 fields of all summer (JJA) blocking days over period of 1955–2024 into twelve different master nodes or patterns, in a configuration of 3 rows by 4 columns, as done in Luu *et al* (2024). The SOM is performed over a domain spanning 80° W–20° E and 40° N–85° N. We then map all blocking days of each individual month to those master nodes and compute the Euclidean distance (ED) over the SOM domain for each blocking day to assess how much it resembles the master node to which it is assigned. The smaller the ED values are, the more similar the blocking days are compared to their corresponding master nodes. We then pool all ED values of blocking days of each month separately to obtain the distribution of ED values for each of the three summer months. We note that all z500 values of JJA are scaled into a range of 0–1, using a min-max scaler technique (e.g. Kim *et al* 2025) for the SOM fitting and ED calculation.

In addition to SOM analysis, we use a different approach for comparing the temporal development of spatial patterns of blocking events over Greenland during the three summer months. For each event detected following the method described above, we use the GB2 index as a measurement of intensity of every blocking day during that event and extract the maximum value of GB2 for each event. Next, we pick the 20 strongest events based on those peak GB2 values for each month. To facilitate our comparison, we centre each blocking event on the date when GB2 reaches peak value and consider the 3 d before and after that centred date, so that all events being considered have an equal length of 7 d. We note that since the GB2 value is used to measure blocking intensity, all those 20 strongest events for each month can be solely determined by GB2 method itself while the D12 method can also detect most (roughly 70%) of them. Then, to investigate whether and how significantly different those spatial patterns of blocking events in 1 month are from other months, and to complement the analysis of mean pattern comparison, we randomly compare spatial patterns of those 20 strongest blocking events of each of the three months in turn to other two summer months. For each pair of months, we randomly pick one event of 7 d length (as described above) from each month and compute the Pearson pattern correlation coefficient of z500 for each corresponding lag day between the two events. We repeat this sampling procedure 5000 times for each pair of months to obtain its distribution of pattern correlation coefficients. To test whether those differences between each pair of months are significant, we create a reference correlation distribution for each month first by randomly comparing two events from that same month. This step is also repeated 5000 times. Given the chaotic nature of the atmosphere, meaning that we would never observe exactly the same two events, we also remove those coefficient values of 1 resulting from comparing an event to itself during the sampling procedure. The reference correlation distribution for each pair of months is obtained by pooling the reference distribution of those two single months. Finally, we apply the Fisher z-transformation to convert those Pearson correlation coefficient distributions into z-score distributions that approximate normal distributions, and we use Welch's T-test to test how significantly different these z-score distributions are compared to their reference distributions. The results of these analyses are shown in section 3.2.

We use the method from Takaya and Nakamura (2001) to compute the horizontal components of phase-independent WAF ($\boldsymbol{F}$) to analyse how wave energy and momentum associated with Rossby wave are transported on a zonally varying mean flow during Greenland blocking episodes,

$$\boldsymbol{F} = \frac{p}{2|\bar{\boldsymbol{U}}|}\left\{\begin{array}{l} \bar{u}\left(\left(\frac{\partial\psi'}{\partial x}\right)^2 - \psi'\frac{\partial^2\psi'}{\partial x^2}\right) + \bar{v}\left(\frac{\partial\psi'}{\partial x}\frac{\partial\psi'}{\partial y} - \psi'\frac{\partial^2\psi'}{\partial x\partial y}\right) \\ \bar{u}\left(\frac{\partial\psi'}{\partial x}\frac{\partial\psi'}{\partial y} - \psi'\frac{\partial^2\psi'}{\partial x\partial y}\right) + \bar{v}\left(\left(\frac{\partial\psi'}{\partial y}\right)^2 - \psi'\frac{\partial^2\psi'}{\partial y^2}\right) \end{array}\right\} + \boldsymbol{C_U M}$$

where $\boldsymbol{U}(u, v)$ is horizontal wind, p denotes pressure normalised by 1000 hPa, ψ is stream function. $\boldsymbol{C_U}$ is wave-phase speed in the direction of **U** flow, and M denotes pseudo-momentum of wave-activity. Overbar denotes climatology mean and prime denotes deviation of variables from background state of the 31 d running mean value centred at the day being considered. We also apply an 8 d low-pass filter

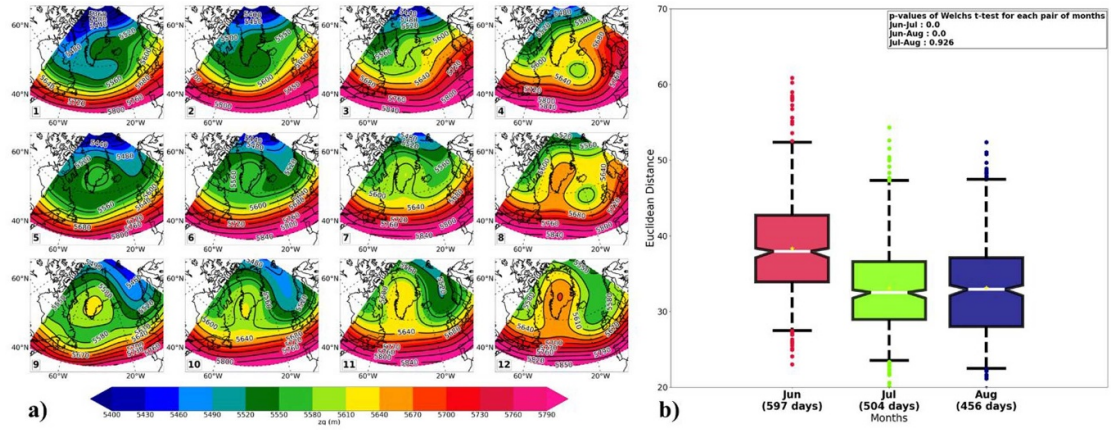

Figure 2. Master SOM patterns of z500 from ERA5 (a) and Euclidean distance distributions (b) between blocking days of each month in comparison with their corresponding master SOM nodes. Weich's *T*-test is used to test the statistical significance of how different ED distribution among the 3 months are. The boxes show interquartile range, the two whiskers mark 2.5th and 97.5th percentiles and the points are outliers.

to the stream function to isolate the quasi-stationary eddies associated with Rossby waves and blocking ridges, and to remove high-frequency transient eddies before computing the anomalies. Therefore, the term associated with phase speed $\boldsymbol{C_U}$ can be neglected (Nishii *et al* 2011).

3. Results

3.1. SOM analysis for individual blocking days

The SOM master nodes and the results of those ED distributions as described in section 2 for all months are shown in figure 2. Although we use a different period of ERA5 data in this study, the results of SOM master nodes agree well with what was found in Luu *et al* (2024). The distribution of ED of July and August are comparable in terms of magnitude, while ED of June is slightly shifted to higher values by roughly 15%, suggesting that June blocking patterns diverge more from the master SOM nodes. We then evaluate the significance of difference of the mean of ED distributions from each pair of months by using the Welch's *T*-test, which does not require the assumption of equal variances between distributions. The results indicate that ED distribution of June is statistically and significantly different (*p*-values close to 0) from those of July and August, while July and August ED distributions are not significantly different. This suggests that the spatial patterns of individual blocking days are more similar for July and August than for June, since they show smaller distances to master nodes. Accordingly, the SOM algorithm puts more weights to blocking days from July and August due to the fact that input samples from those 2 months are identically distributed and they account for almost two thirds of the sample. We also carried out further tests by fitting SOM to blocking days of each individual month separately (figure not shown here) and found that the June ED distribution is closer to those of July and August in this setup. This supports the point that blocking patterns in June are different, to some extent, from those in July and August and less well mapped to the master SOM nodes of JJA. In addition, the standard deviation of z500 field for all blocking days of each month show that June patterns are more variable, with 10–20 m higher in deviation, than July and August, and this high variation extends further south (around 40° N) compared to July and August (around 50° N similarly between the 2 months, figure S2 in supplementary). Although the variation of z500 of each month during non-blocking days is smaller than during blocking days in the same month, the difference of spatial patterns of variation of June compared to July and August remains similar for both blocking and non-blocking days (figure S3 in supplementary). These findings are consistent with the findings of Banderier *et al* (2025) that the patterns of the eddy-driven jet over the North Atlantic and the subtropical jet at lower latitudes during early June are more variable and are not observed in July and August. In addition, these authors show that June is a transition month when the speed of both jets starts to increase and their positions start to shift poleward during June, and the frequency of occurrence of the double jet structure reduces by the end of June.

3.2. Spatial patterns of Greenland blocking

In this section, we first investigate the development of spatial patterns of Greenland blocking for each individual month. Figure 3(a) shows composite plots for the mean of the 20 strongest blocking events over Greenland for June, July, and August (from left to right columns, respectively) from lag −3 to lag 2. We apply a 5 d running mean to filter out the noise for each lag day. In general, a blocking high seems to settle over Greenland from lag −2 for all three months and the Pearson's pattern correlations (applied over the same SOM domain), which measure how the two fields co-vary spatially, at corresponding lag times for each pair of months are large. Spatial patterns of July and August events are constantly and strongly correlated during all lag days, having correlation coefficients ∼0.97, while pattern correlations of each of those two months with June are slightly less strongly correlated ($r \sim 0.9$) as shown in figure 3(b). For June (left column in figure 3), cyclonic Rossby wave breaking together with a ridge retrograding from the British Isles towards Greenland is noticeable during lag −3. The block is well settled over the southern part of Greenland from lag −2 and last until and including lag 2, with a strong negative PV anomaly continuously injected into blocking area from the south-east, as part of the wave breaking. Simultaneously, a cutoff low also develops at lower latitudes south of the southern tip of Greenland, seen in positive PV anomalies and a closed z500 contour. This low feature is not observed for July and August (middle and right columns in figure 3, respectively).

For July, low PV anomaly air starts to develop over Greenland from Iceland and from the southwest of Greenland at lag −3 (figure 3). A ridge then develops from the Atlantic toward Greenland at lag −2, then intensifies until lag 0 before it starts to decay from lag 2. For August, a sign of a ridge developing over northern Norway is visible from lag −3 through z500 patterns with accompanying negative PV anomaly. However, this pattern is not associated with a wave breaking event that facilitates the retrograding of the ridge. At the same time, a negative PV anomaly also develops from the southwest of Greenland, similarly to July's events. Then, a ridge develops from the north Atlantic toward the southern tip of Greenland and its negative PV anomaly merges with the anomaly moving westward from Scandinavia to form a blocking area over Greenland in lag −2. This system is intensified by a stronger negative PV anomaly and is stationary over the same region until lag 2. We note that retrograding ridges from northern Europe are sometimes considered precursors of Greenland blocking in the winter, but these are often less clear than Rossby wave propagating signals coming across North America from the Pacific region toward the area upstream of the blocking region (Woollings *et al* 2008, Parker *et al* 2018).

We then investigate how significant those spatial patterns of blocking events from 1 month are different from other months by randomly sampling and comparing events for each pair of months as described in section 2. The results are shown in box plots in figure 4. The correlation distributions of Jun-Jul and Jun-Aug receive comparable z-scores and the main statistics of the distributions (e.g. mean, median and interquartile) are lower than those of the z-scores distribution of Jul–Aug. This suggests that spatial patterns of strong Greenland blocking events in July and August are correlated to a higher extent than those in June. The p-values from Welch's T-test also show that the correlation distributions of Jun-Jul and Jun-Aug are significantly different from their reference distributions, while that of Jul–Aug is similar to its reference distributions. This means that the spatial correlation of z500 patterns when comparing July and August strong blocking events is not significantly different from comparing strong blocking events drawn from the same month.

3.3. WAF propagation

To gain further insight on what potentially causes the difference in Greenland blocking patterns among summer months, we analyse the phase-independent WAF, which represents how energy and pseudo-momentum are transported, associated with Rossby wave packets over the course of blocking high events. Figure 5 illustrates the development of horizonal (WAFs, vectors) and their horizontal divergence (shaded colours with orange showing convergence and light blue showing divergence) on the 300 hPa surface averaged over the 20 strongest blocking events for the three summer months. The horizontal components of WAF show quasi-stationary features over the course of Greenland blocking events for all three months. For June (left column in figure 5), horizontal WAF sustains around the mid-latitude northern hemisphere (though the Pacific side is not shown in the plot) and stronger than other months and are intensified over Greenland blocking high anomaly region, even from lag −3. Focusing on June, we can also denote an overturning contour line of geopotential height at lag −3 (around the southern tip of Greenland), suggesting the dominance of Rossby wave breaking feature for 20 strongest June events. The wave breaking on this level is in line spatially with what happens on the 500 hPa level (in figure 3) and hence shows minimal vertical tilt between those levels. This suggests that barotropic wave dynamics might strongly influence those events. We also notice that WAF converges horizontally

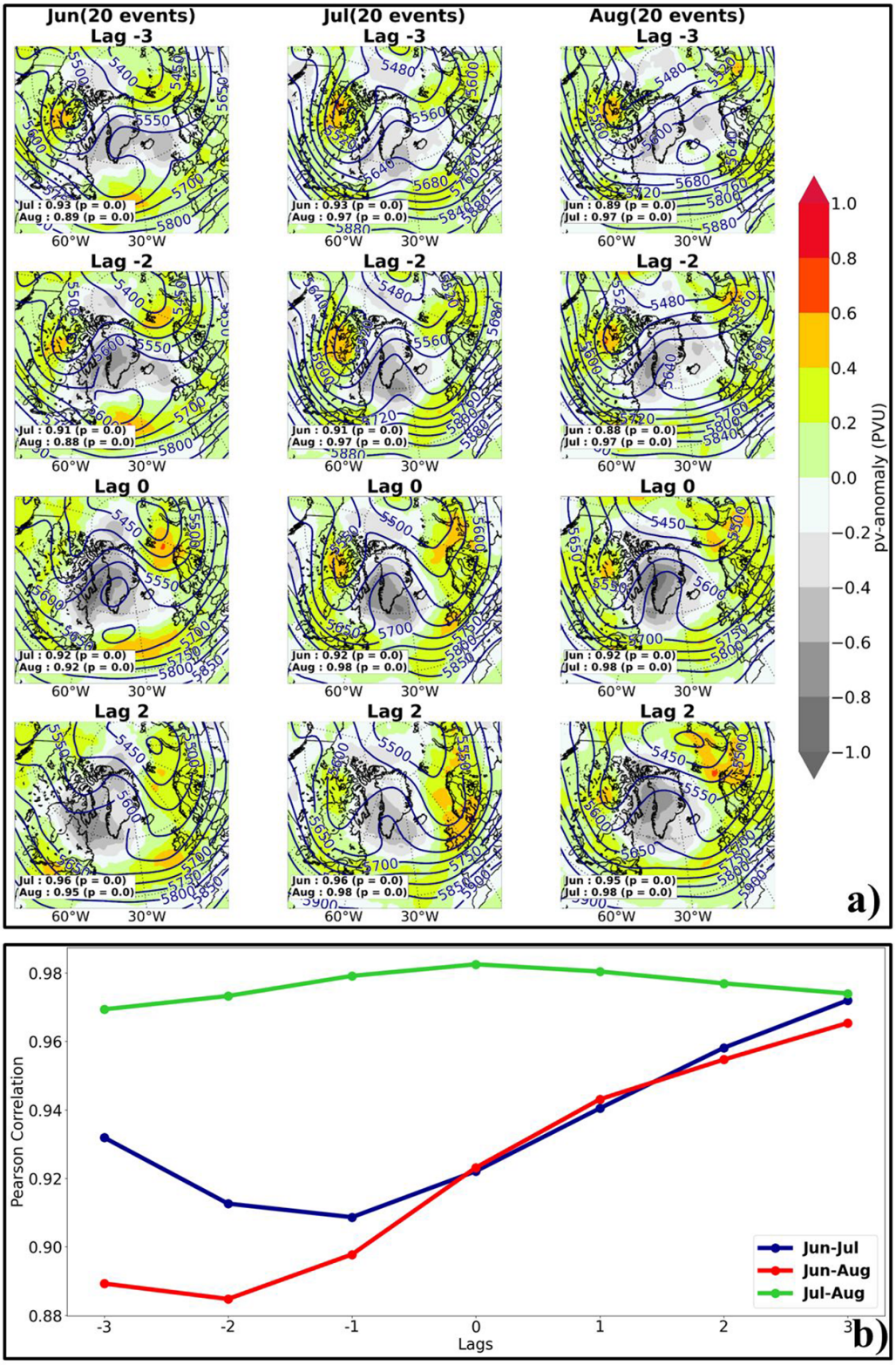

Figure 3. (a) Composite plot showing the mean of the 20 strongest Greenland blocking events for June, July and August (from left to right columns) over the period 1955–2024 from ERA5. Each event is centred on the day when GB2 reaches its peak value over the course of that event. Different rows show different time lags from 3 d before (−3) to 2 d after (+2) the peak day. Contours show z500 and shaded colours show potential vorticity (PV) anomalies averaged over the upper part of the troposphere between 500 and 150 hPa. All lag days are smoothed by a 5 d running mean centred on each of those lag days. The legend on bottom left of each panel shows Pearson's pattern correlation of z500 with *p*-value given in bracket of that time lag of a month to corresponding lag of other months. (b) Pearson correlations for each pair of months as a function of lag days.

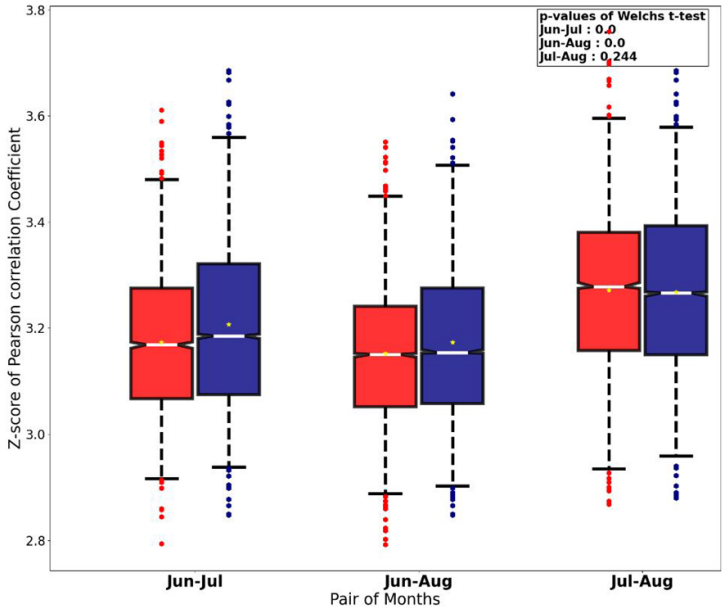

Figure 4. *Z*-score distributions derived from transforming Pearson correlation patterns of blocking events for each pair of months (red box) and their reference distributions (navy box). Welch's *T*-test is used to test the statistical significance of how different ED distribution of each pair of months are from their reference distributions. The boxes show the interquartile range, the two whiskers mark the 2.5th and 97.5th percentiles, and the points are outliers.

upstream, under and even downstream of the blocking ridge for days until it reaches maximum intensity and largely diverges downstream of the block after that day. There is particularly strong convergence of WAF co-located with the cyclonic wave-breaking at lag −3. In addition, during lag 0, the large-scale wave breaks anticyclonically, but this is not observed at lower levels, e.g. 500 hPa. This could potentially be a part of subsequent wave-breaking events that helps to maintain the block against the westerly flow by sustained convergence WAF upstream of the anticyclone. In July and August, WAF converges upstream of the block from lag −3 to lag 0 and diverges strongly at lag 2. To summarise, compared to July and August the June events show stronger wave activity in the region of the block and in the storm track to the south, and have a clear link to the wave-breaking structure.

3.4. Discussion

We show in our study that a retrograding ridge pattern associated with cyclonic wave breakings tends to dominate over the 20 strongest Greenland blocking events in June, whilst an intensified ridge is more common pattern for the strongest events in July and August. The two pathways, called 'retrogression' and 'upstream', respectively, have been discussed in Hauser *et al* (2024) who found that negative PV anomaly air originates from North America and the North Atlantic a few days before blocking onset for both pathways. The negative PV air moves upstream of the block region in the latter pathway, while it propagates toward Europe before retrograding westward and is associated with cyclonic Rossby wave breaking in the former pathway. This westward propagation of negative PV air is supported by moist processes or baroclinicity on the west flank of the blocking anomaly in addition to quasi-barotropic Rossby wave dynamics. Teubler *et al* (2023) also discuss that the retrogression pathway is dominated by eddy fluxes especially before the onset, and this is similar for other blocking regimes over Europe and the North Atlantic. However, notably we bear in mind that for summer blocking the contribution to energy sources of feedback from high-frequency eddies is as important as baroclinic energy conversion from the mean flow (Martineau *et al* 2022).

The evolution of blocking events before their peak days in June is associated with strong convergence of WAF (figure 5). The convergence of WAF coincides with variation of the tendency of density of wave activity pseudo-momentum and is equivalent to the anomalous PV flux without any phase averages (Shi and Nakamura 2021, Shen *et al* 2023). A blocking pattern is usually accompanied by a negative PV flux on the upstream side and a positive PV flux on the downstream side. When the negative PV flank of the block is strengthened by the accumulation of WAF, the block can retrograde westwards in association with Rossby wave breaking (Shi and Nakamura 2021). On the other hand, a strong horizontal shear of negative PV flux can also feedback by enhancing momentum transport and strengthening the ageostrophic flux component, both of which would replenish wave activity upstream of the blocking

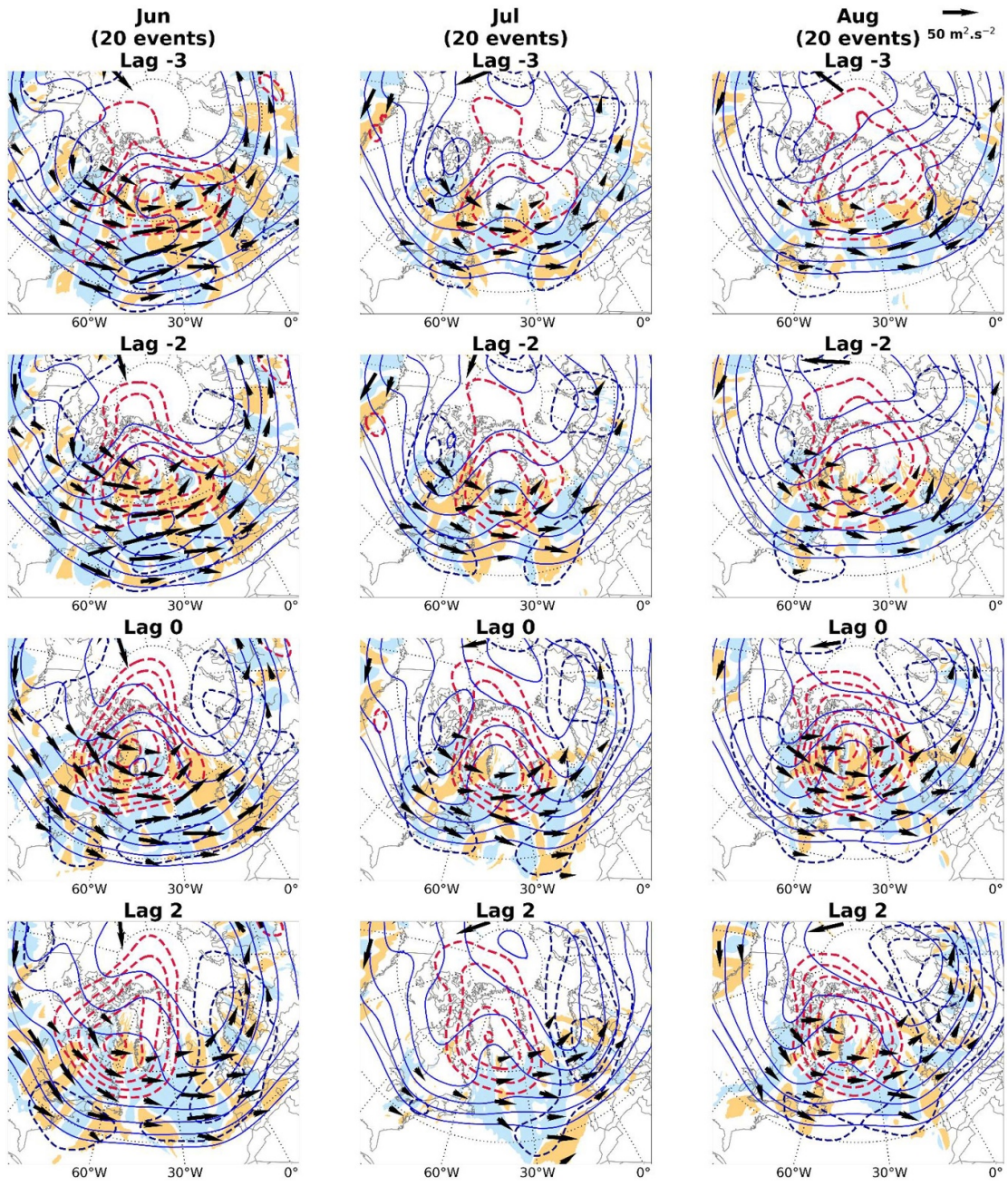

Figure 5. Composite plot of the mean of the 20 strongest blocking events for June, July and August (from left to right columns, respectively) from ERA5. Vectors are horizontal wave activity flux (WAF); blue solid contour shows geopotential height (z300), red (navy) dashed contour shows positive (negative) anomalies of z300, and shaded colour shows horizontal divergence of WAF (orange for convergence and light blue for divergence). All plots are shown for the 300 hPa level.

region (Lojko *et al* 2025). Therefore, apart from the potential interaction with moist processes and baroclinicity as discussed previously, a stronger WAF observed in June could partially explain the dominant cyclonic wave breaking over the eastern Atlantic and western Europe. As suggested in figure S8, a merging jet structure of the subtropical and eddy-driven jets over the North Atlantic is prevailing in June, while the sub-tropical jet is weakening in July and August (as in Banderier *et al* 2025) that is in line with the weakening of the Hadley Cell. That merging jet structure in the June background flow creates a broader waveguide compared to a narrower and more zonal one facilitated by only the eddy-driven jet in July and August. As a result, Rossby wave propagation in June is more prone to wave-breaking patterns. In addition, the subtropical jet in June is stronger and displaced equatorward around the hemisphere, which likely facilitates teleconnection of tropical signals, including from the Asia and Pacific sector, to the North Atlantic via the waveguiding mechanism (Moon *et al* 2013, Branstator and Teng 2017) that enhance the WAF in the region.

Exceptional melt events over GrIS in summer and their increasing trend are highly correlated with atmospheric blocking activity due to surface albedo feedback associated with reduced summer snowfall, enhancing clear-sky downwelling longwave radiation and solar radiation absorption, and the northward development of warm and moist air from lower latitude regions (Tedesco *et al* 2013, Scambos *et al* 2021, Blau *et al* 2024). The amount of surface melt in summer accounts for roughly 90% of annual melt quantities, with July contributing approximately half of summer melt while June and August fractions are relatively similar over the period of 1958–2023 (Zhang *et al* 2025). Zhang *et al* (2025) also show that most of the surface melt happens over the southern ablation areas along the edge of the GrIS. However, there is a significantly increasing contribution from the northern parts of the ice sheet (Noël *et al* 2019, Mattingly *et al* 2023). These differences may partly be due to different anticyclonic patterns persisting during the process. Preece *et al* (2022) suggest that a cyclonic wave-breaking pattern produces more surface melt over the northeast, while omega block and north Atlantic ridge types cause more melt in the north and the south of Greenland, respectively. Tedesco and Fettweis (2020) show that the melt event in summer 2012 was larger than that in 2019, despite the higher temperature anomaly of free atmosphere in 2019, due the difference in blocking patterns. The 2012 event developed from a North Atlantic ridge that was associated with southerly warm and wet air flow facilitating liquid water cloud formation that enhanced surface melt in the dry snow zone. Meanwhile, the 2019 event was characterised by a retrograding ridge from Europe whose lower part of the air mass cooled down over the North Atlantic, which hindered cloud formation.

The coupling relationship between Greenland blocking and the negative phase of the NAO is, albeit not as strong as in the winter, evident in the summer (Woollings *et al* 2008, Folland *et al* 2009, Hanna *et al* 2016). Synoptic-scale wave breaking, a precursor of Greenland blocking, plays an important role in the development of the NAO. Specifically, a single cyclonic wave breaking over the North Atlantic can facilitate the development of the negative phase of the summer NAO (Benedict *et al* 2004, Feldstein 2007). This suggests that the predominant cyclonic wave-breaking preceding Greenland blocking events in June could initiate the difference in the evolution of the NAO between June and July-August. However, the relation among the NAO, wave breaking over the North Atlantic and Greenland blocking as an intermediate in the summer remains uncertain and needs further research to establish the mechanism. In addition to the potential impact on the NAO, we analyse here the downstream impacts of Greenland blocking development on western Europe. Figure 6(a) shows the mean precipitation anomalies for different lag days of Greenland blocking for the 20 strongest events. Each lag day is also smoothed by a 5 d running mean centred on each lag day. Overall, due to the development of wave breaking over northwest of Europe for the June events, a drier than normal pattern is witnessed in this region, especially over the UK, Iceland and northern France from lag −3 and −2. From lag 0 to lag 2, it is slightly wetter in the southern UK and northern France when the blocking high retrogrades towards Greenland. In contrast, it is much wetter over western Europe during July and August Greenland blocking events for all lag days due to the extension further south of the trough downstream of the blocking region. The results from the pattern correlation for each pair of months also show that the downstream impact of Greenland blocking on western European precipitation during July and August are more alike compared to in June, especially from the peak-day onward figure 6(b).

The results we present in section 3 focus on the 20 strongest blocking events of each month because we emphasise the most distinct features which potentially lead to high-impacts over the North Atlantic region. However, to put these main results in a broader perspective, we repeat all analyses from figure 3 to figure 6 on the impact for all blocking events in each month (see figures S4–S7 in the supplementary). In general, the mean patterns of blocking events for different lags in each month show high pattern correlations for both the 500 hPa and 300 hPa levels because the mean patterns are smoothed out in a larger sample. However, we can still denote a sign of cyclonic Rossby wave breaking at 500 hPa during lag −2 for June events that is not noticeable during other months (figure S4). The random sampling comparison for all blocking events (figure S5) also shows similar results as in figure 4, i.e. that blocking events in June are significantly different from those in July and August. In addition, we apply the analysis to an extended summer, i.e. May and September included (figure S4). This shows that Greenland blocking patterns in different months are significantly different, except the pair of July and August. The downstream impact of Greenland blocking on northwest Europe also shows similar features when considering all blocking events instead of only the 20 strongest events (figure S7).

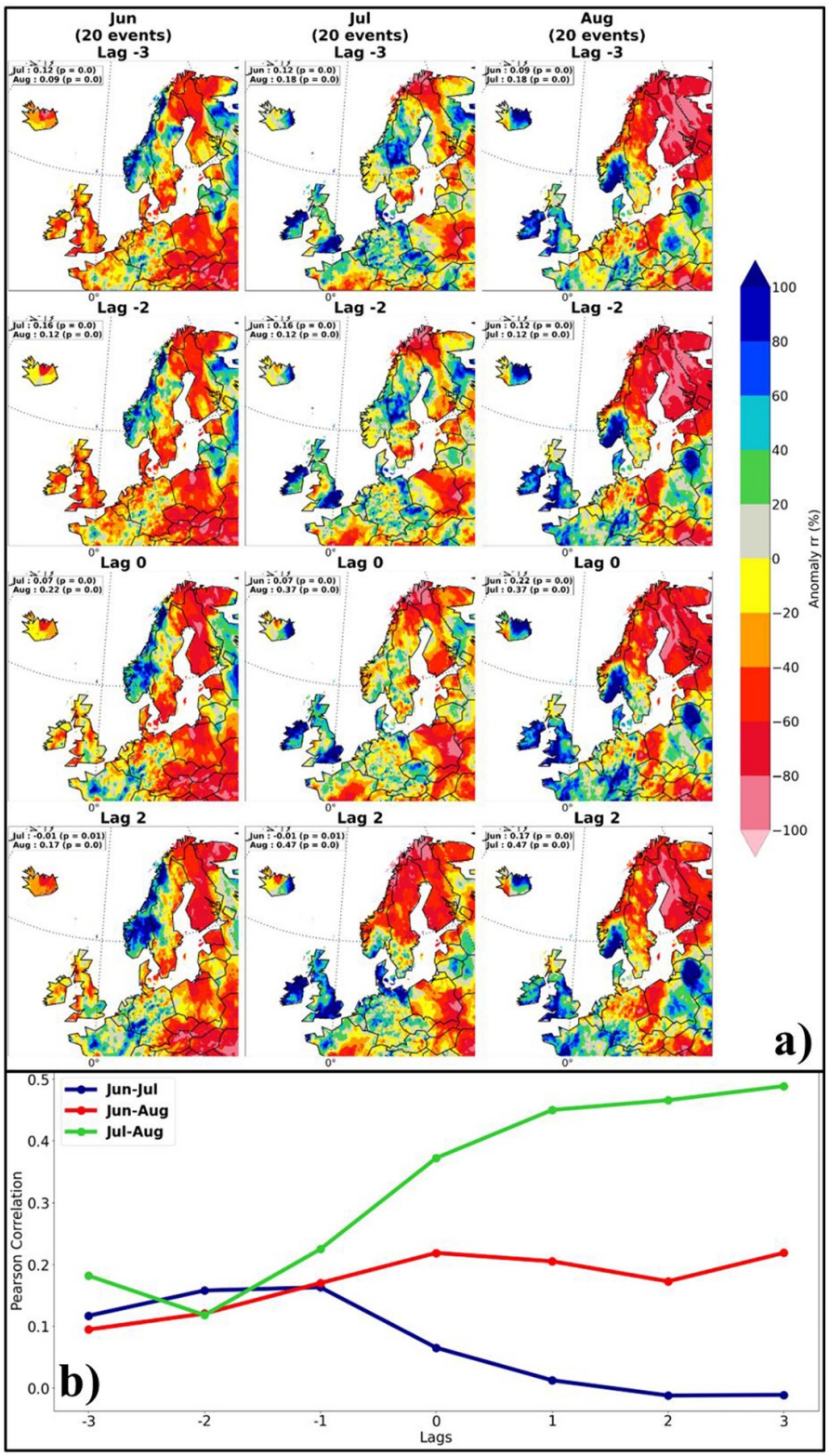

Figure 6. (a) Composite plot of precipitation anomalies of the mean of the 20 strongest blocking events for June, July and August (from left to right columns, respectively) from E-OBS database. All lag days are smoothed by a 5 d running mean centred on each of those lag days. (b) Pearson correlations for each pair of months as a function of lag days. Note that since E-OBS only covers mainland of Europe, we compute the correlation for the domain covering western Europe only (as shown in panel (a)) rather than using the SOM domain as done in the previous section.

4. Conclusions

In this study, we examine the spatial patterns of Greenland blocking among the three summer months for the period of 1955–2024 based on ERA5 reanalysis. We use two different metrics to evaluate the similarity/difference of spatial patterns of blocking events among those three months: a clustering analysis

using a SOM with ED and cross-validation of random-sampling using Pearson pattern correlation for the 20 strongest Greenland blocking events for each month. Together these analyses show a statistically significant difference in the horizontal patterns and evolution of blocking highs in June in comparison with July and August. Blocking events in all three months tend to have an omega shape when they are settled over Greenland on their peak days (i.e. GB2 values reaching highest magnitude), and then slightly retrograde westward on the subsequent days of their decay stage. However, blocking events in June are predominantly associated with cyclonic Rossby wave breaking, whilst blocking events in July and August preferentially develop from an intensified ridge over the North Atlantic. The analyses of all individual blocking events for each month also show similar conclusions to what we find when using only the 20 strongest events.

We also find that all months exhibit quasi-stationary Rossby wave propagation measured by 8 d low-pass filter wind fields in associated with Greenland blocking. In addition, WAF analyses reveal the development of blocking with WAF accumulation of wave energy and pseudo-momentum upstream of the block during build-up period and release of WAF downstream from the peak day onward. The intensity of those fluxes in June events is stronger and more expansive spatially along the mid-latitude regions probably due to its association with a stronger mean flow and the merging of subtropical and eddy-driven jets over the North Atlantic in June. This merged structure creates a broader waveguide and facilitates teleconnection of the North Atlantic with Rossby wave sources in the tropics, which could explain the dominance of Rossby wave breaking as an onset mechanism for blocking events in June. We also find that the downstream impact of Greenland blocking is different for June events with drier than normal conditions observed over the UK and Iceland, while it is wetter than normal for events in July and August.

Acknowledgments

We acknowledge NERC Grant Number NE/W005875/1, and Sergey Chulkov for helpful advice on using the University of Lincoln High Performance Computing cluster on which all analyses in this study are carried out. ERA5 dataset is provided by Copernicus Climate Change Service, Climate Data Store, (2023): ERA5 hourly data on single levels from 1940 to present. Copernicus Climate Change Service (C3S) Climate Data Store (CDS). DOI: 10.24381/cds.adbb2d47. We acknowledge the E-OBS dataset version 31.0e from the EU-FP6 project UERRA (www.uerra.eu) and the Copernicus Climate Change Service, and the data providers in the ECA&D project (www.ecad.eu).

Data availability statement

The data that support the findings of this study are openly available at the following URL/DOI: https://doi.org/10.24381/cds.adbb2d47 (Climate Data Store 2023).

Supplementary figures available at https://doi.org/10.1088/2752-5295/ae71fc/data1.

Author contributions

Edward Hanna 0000-0002-8683-182X
Conceptualization (supporting), Funding acquisition (lead), Investigation (supporting), Methodology (supporting), Supervision (lead), Validation (supporting), Writing – review & editing (supporting)

Tim Woollings
Conceptualization (supporting), Funding acquisition (supporting), Investigation (supporting), Methodology (supporting), Validation (supporting), Writing – review & editing (supporting)

Xavier Fettweis
Funding acquisition (supporting), Methodology (supporting), Writing – review & editing (supporting)

James A Screen 0000-0003-1728-783X
Conceptualization (supporting), Formal analysis (supporting), Funding acquisition (lead), Methodology (supporting), Writing – review & editing (supporting)

Stephanie Hay 0000-0003-4007-842X
Methodology (supporting), Writing – review & editing (supporting)

Jennifer Catto
Funding acquisition (supporting), Methodology (supporting), Writing – review & editing (supporting)

References

Altenhoff A M, Martius O, Croci-Maspoli M, Schwierz C and Davies H C 2008 Linkage of atmospheric blocks and synoptic-scale Rossby waves: a climatological analysis *Tellus B* **60** 1053–63

Banderier H, Tuel A, Woollings T and Martius O 2025 Seasonal to decadal variability and persistence properties of the Euro-Atlantic jet streams characterized by complementary approaches *Weather Clim. Dyn.* **6** 715–39

Beckmann J and Winkelmann R 2023 Effects of extreme melt events on ice flow and sea level rise of the Greenland Ice Sheet *Cryosphere* **17** 3083–99

Benedict J J, Lee S and Feldstein S B 2004 Synoptic view of the north atlantic oscillation *J. Atmos. Sci.* **61** 121–44

Blau M T, Ha K-J and Chung E-S 2024 Extreme summer temperature anomalies over Greenland largely result from clear-sky radiation and circulation anomalies *Commun. Earth Environ.* **5** 405

Branstator G and Teng H 2017 Tropospheric waveguide teleconnections and their seasonality *J. Atmos. Sci.* **74** 1513–32

Cheung H N, Zhou W, Mok H Y, Wu M C and Shao Y 2013 Revisiting the climatology of atmospheric blocking in the Northern Hemisphere *Adv. Atmos. Sci.* **30** 397–410

Cornes R C, van der Schrier G, van den Besselaar E J M and Jones P D 2018 An ensemble version of the E-OBS temperature and precipitation data sets *J. Geophys. Res. Atmos.* **123** 9391–409

Copernicus Climate Change Service, Climate Data Store (2023): ERA5 hourly data on single levels from 1940 to present Copernicus Climate Change Service (C3S) Climate Data Store (CDS) (https://doi.org/10.24381/cds.adbb2d47)

Davini P, Cagnazzo C, Gualdi S and Navarra A 2012 Bidimensional diagnostics, variability, and trends of Northern Hemisphere blocking *J. Clim.* **25** 6496–509

Delhasse A, Fettweis X, Kittel C, Amory C and Agosta C 2018 Brief communication: impact of the recent atmospheric circulation change in summer on the future surface mass balance of the Greenland ice sheet *Cryosphere* **12** 3409–18

Deshmukh V, Rivière G, Fromang S and Saint-Lu M 2025 How does a dry general circulation model represent atmospheric blocking? *J. Atmos. Sci.* **82** 283–300

Dong B, Sutton R T, Woollings T and Hodges K 2013 Variability of the North Atlantic summer storm track: mechanisms and impacts on European climate *Environ. Res. Lett.* **8** 034037

Drouard M and Woollings T 2018 Contrasting mechanisms of summer blocking over Western Eurasia *Geophys. Res. Lett.* **45** 12,040–8

Drouard M, Woollings T, Sexton D M H and McSweeney C F 2021 Dynamical differences between short and long blocks in the Northern hemisphere *J. Geophys. Res. Atmos.* **126** e2020JD034082

Dunstone N *et al* 2023 Skilful predictions of the summer North Atlantic oscillation *Commun. Earth Environ.* **4** 409

Elliott R D and Smith T B 1949 A study of the effects of large blocking highs on the general circulation in the Northern-hemisphere westerlies *J. Meteorol.* **6** 68–85

Feldstein S B 2007 The dynamics of the North Atlantic oscillation during the summer season *Q. J. R. Meteorol. Soc.* **133** 1509–18

Fettweis X, Franco B, Tedesco M, van Angelen J H, Lenaerts J T M, van den Broeke M R and Gallée H 2013 Estimating the Greenland ice sheet surface mass balance contribution to future sea level rise using the regional atmospheric climate model MAR *Cryosphere* **7** 469–89

Folland C K, Knight J, Linderholm H W, Fereday D, Ineson S and Hurrell J W 2009 The summer North Atlantic oscillation: past, present, and future *J. Clim.* **22** 1082–103

Hall R J and Hanna E 2018 North Atlantic circulation indices: links with summer and winter UK temperature and precipitation and implications for seasonal forecasting *Int. J. Climatol.* **38** e660–77

Hanna E *et al* 2024 Influence of high-latitude blocking and the northern stratospheric polar vortex on cold-air outbreaks under Arctic amplification of global warming *Environ. Res.: Clim.* **3** 042004

Hanna E, Cropper T E, Hall R J and Cappelen J 2016 Greenland blocking index 1851–2015: a regional climate change signal *Int. J. Climatol.* **36** 4847–61

Hanna E, Hall R J, Cropper T E, Ballinger T J, Wake L, Mote T and Cappelen J 2018 Greenland blocking index daily series 1851–2015: analysis of changes in extremes and links with North Atlantic and UK climate variability and change *Int. J. Climatol.* **38** 3546–64

Hanna E, Hall R J and Overland J E 2017 Can Arctic warming influence UK extreme weather? *Weather* **72** 346–52

Hauser S, Teubler F, Riemer M, Knippertz P and Grams C M 2023 Towards a holistic understanding of blocked regime dynamics through a combination of complementary diagnostic perspectives *Weather Clim. Dyn.* **4** 399–425

Hauser S, Teubler F, Riemer M, Knippertz P and Grams C M 2024 Life cycle dynamics of Greenland blocking from a potential vorticity perspective *Weather Clim. Dyn.* **5** 633–58

He Y, Huang J, Li D, Xie Y, Zhang G, Qi Y, Wang S and Totz S 2018 Comparison of the effect of land-sea thermal contrast on interdecadal variations in winter and summer blockings *Clim. Dyn.* **51** 1275–94

Hermann M *et al* 2020 A Lagrangian analysis of the dynamical and thermodynamic drivers of large-scale Greenland melt events during 1979–2017 *Weather Clim. Dyn.* **1** 497–518

Hersbach H *et al* 2020 The ERA5 global reanalysis *Q. J. R. Meteorol. Soc.* **146** 1999–2049

Hoskins B 1997 A potential vorticity view of synoptic development *Meteorol. Appl.* **4** 325–34

Kautz L-A, Martius O, Pfahl S, Pinto J G, Ramos A M, Sousa P M and Woollings T 2022 Atmospheric blocking and weather extremes over the Euro-Atlantic sector—a review *Weather Clim. Dyn.* **3** 305–36

Kim Y-S, Kim M K, Fu N, Liu J, Wang J and Srebric J 2025 Investigating the impact of data normalization methods on predicting electricity consumption in a building using different artificial neural network models *Sustain. Cities Soc.* **118** 105570

Liu J, Chen Z, Francis J, Song M, Mote T and Hu Y 2016 Has Arctic sea ice loss contributed to increased surface melting of the greenland ice sheet? *J. Clim.* **29** 3373–86

Lojko A, Winters A C, Oertel A, Jablonowski C and Payne A E 2025 An ERA5 climatology of synoptic-scale negative potential vorticity–jet interactions over the western North Atlantic *Weather Clim. Dyn.* **6** 387–411

Luo D 2000 Planetary-scale baroclinic envelope Rossby solitons in a two-layer model and their interaction with synoptic-scale eddies *Dyn. Atmos. Oceans* **32** 27–74

Luo D, Zhang W and Luo B 2025 A nonlinear multi-scale interaction model for atmospheric blocking: a tool for exploring the impact of changing climate on mid-to-high latitude weather extremes *Adv. Atmos. Sci.* **42** 2018–35
Lupo A R 2021 Atmospheric blocking events: a review *Ann. New York Acad. Sci.* **1504** 5–24
Lupo A R, Jensen A D, Mokhov I I, Timazhev A V, Eichler T and Efe B 2019 Changes in global blocking character in recent decades *Atmosphere* **10** 92
Lupo A R and Smith P J 1995 Climatological features of blocking anticyclones in the Northern Hemisphere *Tellus A* **47** 439–56
Luu L N, Hanna E, de Alwis Pitts D, Maddison J, Screen J A, Catto J L and Fettweis X 2024 Greenland summer blocking characteristics: an evaluation of a high-resolution multi-model ensemble *Clim. Dyn.* **62** 10503–23
Ma J and Liang X S 2023 Upstream–downstream asymmetry in multiscale interaction underlying the Northern hemisphere atmospheric blockings *J. Atmos. Sci.* **80** 1995–2011
Martineau P, Nakamura H, Yamamoto A and Kosaka Y 2022 Baroclinic blocking *Geophys. Res. Lett.* **49** e2022GL097791
Mathews J and Czaja A 2024 Oceanic maintenance of atmospheric blocking in wintertime in the North Atlantic *Clim. Dyn.* **62** 6159–72
Mattingly K S, Mote T L and Fettweis X 2018 Atmospheric river impacts on Greenland ice sheet surface mass balance *J. Geophys. Res. Atmos.* **123** 8538–60
Mattingly K S, Turton J V, Wille J D, Noël B, Fettweis X, Rennermalm Å K and Mote T L 2023 Increasing extreme melt in northeast Greenland linked to foehn winds and atmospheric rivers *Nat. Commun.* **14** 1743
McLeod J T and Mote T L 2015 Assessing the role of precursor cyclones on the formation of extreme Greenland blocking episodes and their impact on summer melting across the Greenland ice sheet *J. Geophys. Res. Atmos.* **120** 12357–77
McLeod J T and Mote T L 2016 Linking interannual variability in extreme Greenland blocking episodes to the recent increase in summer melting across the Greenland ice sheet *Int. J. Climatol.* **36** 1484–99
Miller D E and Wang Z 2022 Northern Hemisphere winter blocking: differing onset mechanisms across regions *J. Atmos. Sci.* **79** 1291–309
Moon J-Y, Wang B, Ha K-J and Lee J-Y 2013 Teleconnections associated with Northern Hemisphere summer monsoon intraseasonal oscillation *Clim. Dyn.* **40** 2761–74
Nabizadeh E *et al* 2021 The 3D Structure of Northern Hemisphere blocking events: climatology, role of moisture, and response to climate change *J. Clim.* **34** 9837–60
Nakamura H, Nakamura M and Anderson J L 1997 The role of high- and low-frequency dynamics in blocking formation *Mon. Weather Rev.* **125** 2074–93
Nakamura N and Huang C S Y 2018 Atmospheric blocking as a traffic jam in the jet stream *Science* **361** 42–47
Nishii K, Nakamura H and Orsolini Y J 2011 Geographical dependence observed in blocking high influence on the stratospheric variability through enhancement and suppression of upward planetary-wave propagation *J. Clim.* **24** 6408–23
Noël B, van de Berg W J, Lhermitte S and van den Broeke M R 2019 Rapid ablation zone expansion amplifies north Greenland mass loss *Sci. Adv.* **5** eaaw0123
Parker T, Woollings T and Weisheimer A 2018 Ensemble sensitivity analysis of Greenland blocking in medium-range forecasts *Q. J. R. Meteorol. Soc.* **144** 2358–79
Pelly J L and Hoskins B J 2003 A new perspective on blocking *J. Atmos. Sci.* **60** 743–55
Preece J R, Wachowicz L J, Mote T L, Tedesco M and Fettweis X 2022 Summer Greenland blocking diversity and its impact on the surface mass balance of the Greenland ice sheet *J. Geophys. Res. Atmos.* **127** e2021JD035489
Scambos T, Straneo F and Tedesco M 2021 How fast is the Greenland ice sheet melting? Arctic *Antarct. Alp. Res.* **53** 221–2
Schwierz C *et al* 2004 Perspicacious indicators of atmospheric blocking *Geophys. Res. Lett.* **31**
Sellevold R, Lenaerts J T M and Vizcaino M 2022 Influence of Arctic sea-ice loss on the Greenland ice sheet climate *Clim. Dyn.* **58** 179–93
Shen X, Wang L, Scaife A A, Hardiman S C and Xu P 2023 The stratosphere–troposphere oscillation as the dominant intraseasonal coupling mode between the stratosphere and troposphere *J. Clim.* **36** 2259–76
Shi N and Nakamura H 2021 A new detection scheme of wave-breaking events with blocking flow configurations *J. Clim.* **34** 1467–83
Steinfeld D and Pfahl S 2019 The role of latent heating in atmospheric blocking dynamics: a global climatology *Clim. Dyn.* **53** 6159–80
Sun Y, Simpson I, Wei H-L and Hanna E 2024 Probabilistic seasonal forecasts of North Atlantic atmospheric circulation using complex systems modelling and comparison with dynamical models *Meteorol. Appl.* **31** e2178
Takaya K and Nakamura H 2001 A formulation of a phase-independent wave-activity flux for stationary and migratory quasigeostrophic eddies on a zonally varying basic flow *J. Atmos. Sci.* **58** 608–27
Tedesco M and Fettweis X 2020 Unprecedented atmospheric conditions (1948–2019) drive the 2019 exceptional melting season over the Greenland ice sheet *Cryosphere* **14** 1209–23
Tedesco M, Fettweis X, Mote T, Wahr J, Alexander P, Box J E and Wouters B 2013 Evidence and analysis of 2012 Greenland records from spaceborne observations, a regional climate model and reanalysis data *Cryosphere* **7** 615–30
Teubler F, Riemer M, Polster C, Grams C M, Hauser S and Wirth V 2023 Similarity and variability of blocked weather-regime dynamics in the Atlantic–European region *Weather Clim. Dyn.* **4** 265–85
Vishnupriya S, Sprenger M, Joos H and Wernli H 2025 The interaction of warm conveyor belt outflows with the upper-level waveguide: a four-type climatological classification *Weather Clim. Dyn.* **6** 1195–219
Wachowicz L J *et al* 2020 Historical trends of seasonal Greenland blocking under different blocking metrics *Int. J. Climatol.* **41** E3263–78
Weijenborg C, de Vries H and Haarsma R J 2012 On the direction of Rossby wave breaking in blocking *Clim. Dyn.* **39** 2823–31
Wiedenmann J M, Lupo A R, Mokhov I I and Tikhonova E A 2002 The climatology of blocking anticyclones for the Northern and Southern Hemispheres: block intensity as a diagnostic *J. Clim.* **15** 3459–73
Woollings T, Barriopedro D, Methven J, Son S-W, Martius O, Harvey B, Sillmann J, Lupo A R and Seneviratne S 2018 Blocking and its response to climate change *Curr. Clim. Change Rep.* **4** 287–300
Woollings T and Hoskins B 2008 Simultaneous Atlantic–Pacific blocking and the Northern annular mode *Q. J. R. Meteorol. Soc.* **134** 1635–46
Woollings T, Hoskins B, Blackburn M and Berrisford P 2008 A new rossby wave–breaking interpretation of the North Atlantic oscillation *J. Atmos. Sci.* **65** 609–26
Yeh T-C 1949 On energy dispersion in the atmosphere *J. Atmos. Sci.* **6** 1–16
Zhang C *et al* 2024 Impacts of stratospheric polar vortex changes on tropospheric blockings over the Atlantic region *Clim. Dyn.* **62** 4829–48
Zhang Q-L *et al* 2025 Variations in Greenland surface melt and extreme events from 1958 to 2023 *Adv. Clim. Change Res.* **16** 910–21